Available online at www.sciencedirect.com
SCIENCE DIRECT®
Journal of Nuclear Materials 337–339 (2005) 742–746
journal of nuclear materials
www.elsevier.com/locate/jnucmat

SOL and pedestal density profile evolution during DIII-D ELMy and ELM-suppressed H-mode operation

L. Zeng [a,*], G. Wang [a], E.J. Doyle [a], T.L. Rhodes [a], W.A. Peebles [a], M.E. Fenstermacher [b], T.E. Evans [c], R.A. Moyer [d]

[a] University of California, Los Angeles, CA 90095-1597, USA
[b] Lawrence Livermore National Laboratory, Livermore, CA 94550, USA
[c] General Atomics, San Diego, CA 92186-5608, USA
[d] University of California at San Diego, La Jolla, CA 92093-0417, USA

Abstract

A fast profile reflectometer has been used to study the detailed characteristics of scrape-off-layer (SOL) and pedestal density profile evolution in DIII-D ELMy H-mode plasmas with high temporal ($\geqslant 10$ μs) and spatial (~4 mm) resolution. Results show a significant enhancement in radial particle transport to the outer vessel wall during Type-I ELMs. The radial particle transport time (~140 μs) becomes comparable to the parallel transport time, as a result of a high radial velocity (~620 m/s) of SOL profile expansion. The dynamics can vary from ELM-to-ELM. Scalings with pedestal density have been obtained, indicating that ELM is less affected as the pedestal density increases. Finally, during ELM-suppressed H-mode operation with a stochastic magnetic boundary, the radial extent of observed SOL profile modifications do not extend to the vessel wall, and profiles are steeper, substantially different from the SOL changes associated with Type-I ELMs.

PACS: 52.40.HF; 52.55.Fa; 52.65.−y; 52.70.−m
Keywords: ELM; DIII-D; SOL plasma boundary; Pedestal; Reflectometer

1. Introduction

In high confinement H-mode plasmas, edge localized mode (ELM) instabilities produce transient perturbations of the edge pedestal and scrape-off-layer (SOL), modulating the heat and particle transport into the SOL and divertor [1–6]. In a leading theoretical model for ELMs, the Type-I ELM is driven both by the pedestal pressure gradient and current profile (peeling-ballooning model [3]). However, questions remain concerning the magnitude of the ELM-induced energy and particle pulses leaving the pedestal, the propagation of the pulses from the SOL to the vessel wall, the fraction of ELM particle or energy deposited to the vessel wall, how the deposition scales with plasma parameters, etc. [4]. Consequently, detailed investigation of plasma characteristics in the SOL and pedestal regions remains important for ELM physics understanding.

A fast profile reflectometer with high temporal ($\geqslant 10$ μs) and spatial (~4 mm) resolution [7,8], has been

* Corresponding author. Address: General Atomics, P.O. Box 85608, MS 13-364, San Diego, CA 92186-5608, USA.
E-mail address: zeng@fusion.gat.com (L. Zeng).

0022-3115/$ - see front matter © 2004 Elsevier B.V. All rights reserved.
doi:10.1016/j.jnucmat.2004.09.037

successfully used to measure the SOL and pedestal density profile modifications associated with ELMs in DIII-D [8–10]. The reflectometer system was recently upgraded to expand the measured density range to 0–6.4×10^{19} m^{-3}, with high time resolution, such that the system now has the capability to resolve the whole pedestal profile evolution associated with ELMs. Through the investigation of the time resolved electron density profile modifications, a number of the outstanding ELM physics issues mentioned above have been directly addressed. In addition, reflectometer data have also been used to investigate detailed SOL density profile characteristics during ELM-suppressed operation with a stochastic magnetic boundary, an ELM suppression technique recently developed on DIII-D [11].

2. Fast profile reflectometer system

On DIII-D, both Thomson scattering and profile reflectometer systems provide electron density profile measurements. Normally, Thomson scattering measures a density profile every 12 ms, which is insufficient for ELM evolution studies. The profile reflectometer on DIII-D uses solid-state microwave sources such that the system can be continuously frequency swept full-band in as little as 10 μs, every sweep providing a profile measurement. In a new dual-polarization configuration, probe beams are launched at a 45° polarization into the plasma, so as to couple to both O- and X-mode waves. Use of simultaneous O- and X-mode measurements expands the measured density range, which is now 0–6.4×10^{19} m^{-3}, with no unmeasured density gaps [7].

3. SOL and pedestal density profile evolution associated with ELMs

A detailed example of the density profile evolution through a single Type-I ELM is shown in Fig. 1. The ELM timing is shown by a divertor D_α signal, Fig. 1(a), where the numbers and vertical lines represent the times for the density profile sequence shown in Fig. 1(b). The plasma parameters for this typical ELMing discharge were 1.0 MA, $B_T = 1.7$ T and $T_{e0} = 2.1$ keV, in a lower single null plasma configuration. The pedestal density was 3.2×10^{19} m^{-3}, corresponding to a normalized pedestal density of ~0.3 times the Greenwald density, $n_{GW}(10^{20}\ \mathrm{m}^{-3}) = I_p(\mathrm{MA})/[\pi a^2(\mathrm{m})]$. Under these conditions the reflectometer system can track the complete profile evolution to the top of the pedestal density. In Fig. 1(b), profile 1 is taken just before the ELM onset, and shows a typical steep edge pedestal which defines the H-mode edge barrier region. At the onset of the ELM, profile 2 shows an increase in SOL density, with the density at the top of the pedestal slightly reduced.

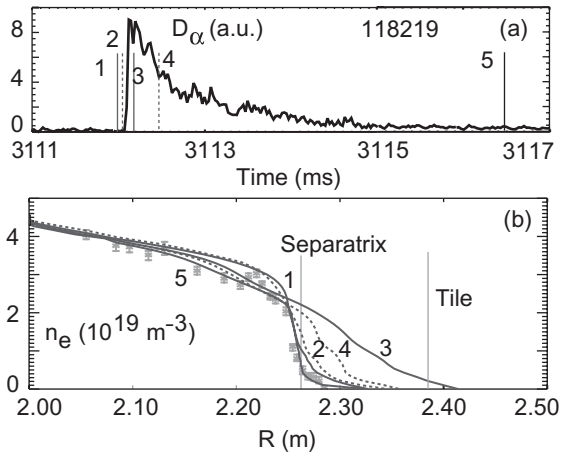

Fig. 1. Profile evolution during a single ELM, showing: (a) divertor D_α signal, where the numbers and vertical lines represent the times for the density profile sequence shown in (b). The points with error bars in (b) are Thomson scattering data taken at the same time as profile 5.

At the time of the ELM crash (1st peak of the D_α profile 3), about 100 μs later, the SOL profile has expanded radially outward to the vessel wall, where there is a relatively large density rise of $\sim2\times10^{18}$ m^{-3}. During the recovery phase, profile 4 shows the pedestal gradually rebuilding, and SOL density reducing. The final profile in the sequence, 5, shows a return to a well defined edge pedestal several ms after the ELM onset. Thomson scattering data obtained at the same time as reflectometer profile 5 are shown via points with error bars, showing good agreement between the two measurements. The illustrated evolution of the pedestal and SOL density profiles demonstrates that the density rise observed in the SOL is directly linked to the pedestal loss during the ELM.

The observed ELM dynamics are shown in more detail in Fig. 2, which shows the density profile evolution through a sequence of three Type-I ELMs. The profile evolution is depicted via contours of constant density as shown in Fig. 2(b), where the density of each numbered contour is marked on a scale, and the density range is 0–4.5×10^{19} m^{-3}. The horizontal solid line represents the midplane separatrix radius, and the ELM timing is again shown by a D_α signal from the divertor, Fig. 2(a). During the ELMs, the SOL profile expands rapidly outwards, as indicated by the movement of contours 1 and 2 in Fig. 1(b). The lowest density contour, shows that the SOL density profile expands out to the outer wall radius (tile radius $R = 2.377$ m). By contrast, the density profile inside the separatrix is flattened and the pedestal transiently eliminated, as indicated by the inward movement of contours 4, 5 and 6 and increased separation from contour 3. The minimal modification of

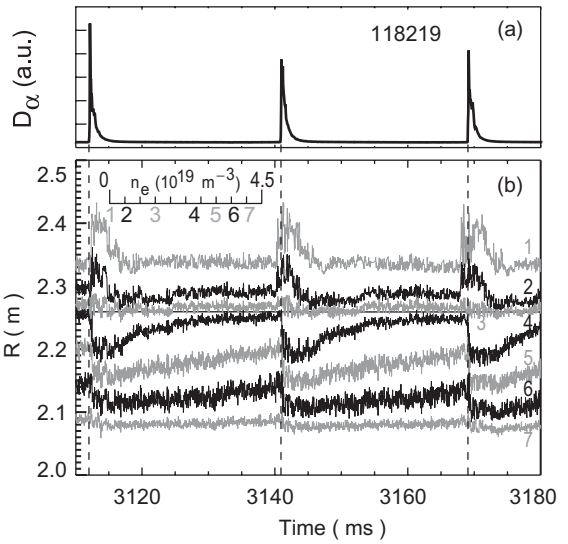

Fig. 2. Time evolution of the SOL and pedestal profile through a sequence of three ELMs, showing: (a) D_α signal, (b) contours of fixed density as a function of radius and time, with 25 μs time resolution, where the labels indicate the different density layers and the horizontal solid line shows the separatrix position.

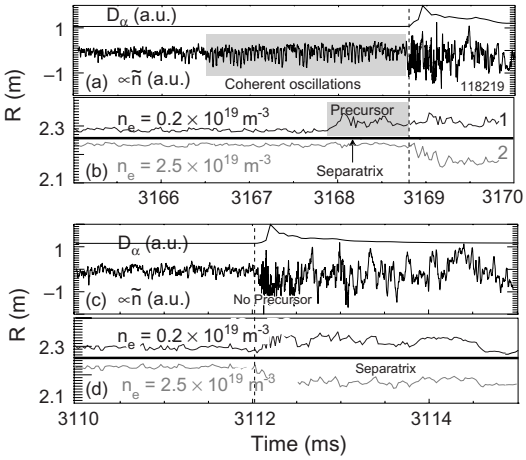

Fig. 3. Detailed comparison of two ELMs, with ((a), (b)) and without ((c), (d)) precursor SOL profile activity. For the first ELM, the SOL density layer (line 1) shown in (b), clearly starts to move radially outwards ~1 ms before ELM onset, while the density layer inside the separatrix (line 2) shows no significant change until ELM onset. A SOL density fluctuation indicates the presence of a growing coherent oscillation for ~2–3 ms before the ELM onset. Comparable data for an ELM without this profile precursor activity are shown in (c) and (d).

contour 7 indicates that the ELM profile modification is edge localized, consistent with previous results from Thomson scattering [12], while contour 3 shows the existence of a density pivot point.

An interesting feature of the data shown in Fig. 2 is the varying dynamics from ELM-to-ELM. Specifically, ELM precursors in the form of changes in the SOL density profile are observed just before ELMs 2 and 3, but not for ELM 1. This precursor in the density profile behavior is localized to the SOL and occurs up to ~1 ms before ELM onset; no ne precursor is observed inside the separatrix. An expanded view of this varying precursor activity is shown in Fig. 3(a) and (b) (with precursor) and (c) and (d) (no precursor). In Fig. 3(a) density fluctuations, which are measured by a 15 GHz O-mode reflectometer at a 2×10^{18} m^{-3} density layer, indicate a growing coherent oscillation (also seen on magnetic probes) for ~2–3 ms before the ELM onset. For this ELM, the SOL density layer at $n_e = 2\times10^{18}$ m^{-3}, Fig. 3(b), clearly starts to move radially outwards ~1 ms before ELM onset, while the $n_e = 2.5\times10^{19}$ m^{-3} density layer, located inside the separatrix shows no significant change until ELM onset. Comparable data for an ELM without this profile precursor activity are shown in Fig. 3(c) and (d). This varying precursor behavior illustrates that ELM dynamics can vary, and is consistent with results reported from JET [13].

The ELM radial propagations with significant velocities have been found in several tokamaks [2,4]. The radial velocity V_r of density layer movement during ELMs can be derived directly from the time resolved profile data; it was previously shown that the radial velocity derived in this manner is in good agreement with Langmuir probe measurements, and consistent with BES measurements [4,14]. At the time of the ELM crash, as indicated by the D_α signal in Fig. 4(a), the radial velocity close to the tile radius is observed to be ~620 m/s, as shown by the dashed line in Fig. 4(b). With this velocity, the radial transport time is ~140 μs, comparable to the parallel transport time, normally ~100 μs in DIII-D[4]. The radial particle flux, $\Gamma = nV_r$, can also be obtained from the time resolved profile data. As shown in Fig. 4(b), the particle flux (solid line) close to the tile radius is $\sim1.5\times10^{21}$ m^{-2} s^{-1} during an ELM crash (at $n_{ped}/n_{GW} = 0.3$ in this case). Since the radial flux at the last closed flux surface is $\sim6.0\times10^{21}$ m^{-2} s^{-1} measured by Langmuir probes [14], a significant particle flux fraction ~25% to the wall illustrates the enhanced particle radial transport due to ELMs. The density scaling of the particle flux as a function of pedestal density was investigated by obtaining a series of discharges with the same B_T, I_p, q and separatrix position, but varying density. The radial particle flux at the time of the ELM crash is plotted as a function of n_{ped}/n_{GW} in Fig. 4(c), the data being averaged over 10 ELMs for each discharge. As can be seen, the particle flux substantially reduces with increasing density. In previous work [9], the normalized density at the vessel wall, and normalized density fluctu-

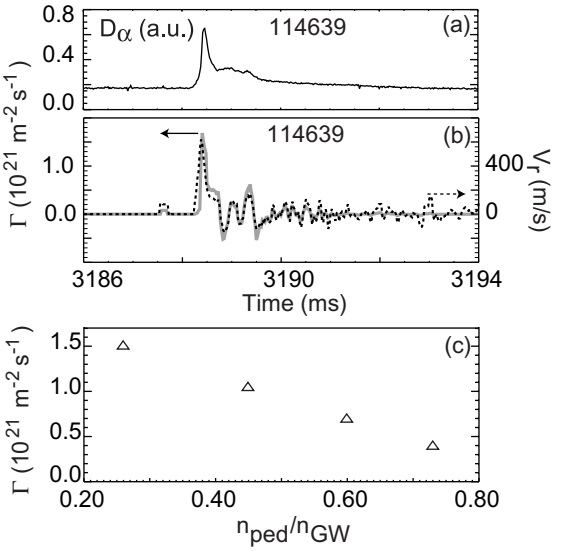

Fig. 4. (a) D_α signal for ELM timing and, (b) radial particle flux, nV_r, and radial velocity of density layers to the outboard midplane tile radius for the same ELM as shown in (a). (c) Scaling of radial particle flux at time of ELM crash with, with data from a sequence of discharges, and averaged over 10 ELMs.

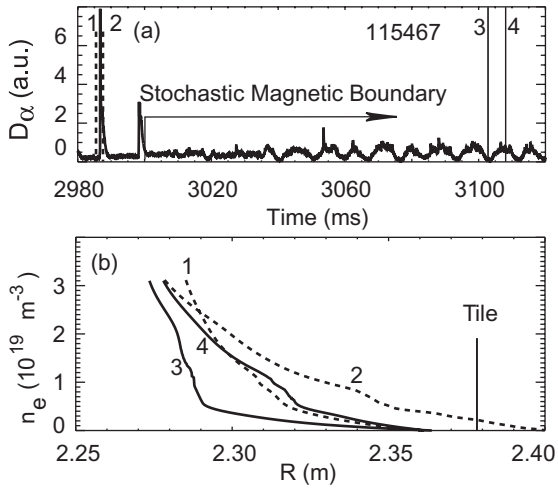

Fig. 5. Profile evolution with and without an ELM-suppressed H-mode. ELM and D_α oscillation timing is indicated in (a), while (b) shows density profiles at four times of interest. Profiles 1 and 2 (dashed lines) indicate the density modification by an ELM, while profiles 3 and 4 (solid lines) show the profile modifications associated with a small D_α oscillation observed during the ELM-suppressed phase.

ation level in the pedestal were also shown to similarly decrease with increasing pedestal density.

4. Edge density profile with a stochastic magnetic boundary

DIII-D has recently demonstrated an ELM suppression technique utilizing a stochastic magnetic boundary produced by an MHD control coil inside the vessel [11]. While the ELMs are suppressed, the H-mode edge can display rapid, small D_α oscillations with a bursty character, modulated by a coherent 200 Hz envelope. Edge density profiles before and after ELM suppression are presented in Fig. 5. Profiles 1 and 2 in Fig. 5(b) are from before and during an ELM, respectively, in the ELMy phase of the discharge, before the stochastic magnetic boundary is formed and ELMs were suppressed. The SOL density profile expands to the tile position during the ELM, consistent with other Type-I ELMs, as discussed above. After the application of the stochastic magnetic boundary and with ELMs suppressed, however, the profiles are distinctly different. Profiles 3 and 4 in Fig. 5(b) show data from different phases of the D_α oscillations observed during ELM suppression. Profile 4, at the maximum of the oscillation amplitude, is broader than profile 3 at the minimum of the oscillation. However, the profile during ELM suppression never expands to the outer midplane tile radius. Also, profiles 3 and 4 show steeper density gradients than profiles 1 and 2, respectively, indicating a change in SOL radial transport due to the stochastic magnetic boundary.

5. Discussion and conclusions

A novel, high-performance fast profile reflectometer system has been used to investigate the detailed evolution of SOL and pedestal density profiles during Type-I ELMs on DIII-D. There is a significant and rapid enhancement in radial particle transport and particle flux to the outer vessel wall during Type-I ELMs, e.g. the particle flux at the outboard midplane tile radius rises $\sim 1.5 \times 10^{21}$ m^{-2} s^{-1}, which is about 25% at LCFS. Also during the ELMs, the radial transport time $\sim$140 μs, is comparable to the parallel transport, as a result of a high radial velocity (up to 620 m/s), with which the SOL profile expands. With some, but not all ELMs, an ELM precursor in the form of a radial expansion in the SOL density profile was observed on a $\sim$1 ms time scale before ELM onset. That such precursors are not always observed is indicative of varying ELM dynamics.

Scalings with pedestal density have been obtained, indicating that ELM effects decrease as the pedestal density increases. Specifically, the normalized density at the vessel wall, particle flux to the wall and normalized density fluctuation level in the pedestal all decrease with increasing pedestal density. Edge stability analysis of ELMs in other, similar, DIII-D discharges using the

ELITE code [15,16], shows that the radial extent of the unstable mode decreases as density increases, indicating ELM strength is diminished at higher density. The results are consistent with the experimental scaling results presented in this paper.

During ELM-suppressed H-mode edge pedestal operation using a stochastic magnetic boundary, the measured density profiles indicate that the radial extent of SOL profile modifications are reduced and do not expand to the midplane tile radius, substantially different from the profile modification observed with large Type-I ELMs. In addition, the SOL profiles are steeper than in the ELMy phase, indicating that the stochastic magnetic boundary affects the particle transport. Such ELM-suppressed operation may offer a promising operating mode for future tokamak reactors.

Acknowledgment

Work supported by US DOE Grant Nos. DE-FG03-01ER54615, DE-FG03-96ER54373, DE-FG03-95ER54294 and Contract Nos. DE-FC02-04ER54698, DE-AC03-89ER51114, W-7405-ENG-48.

References

[1] H. Zohm, Plasma Phys. Control. Fusion 38 (1996) 105.
[2] B. Goncalves et al., Plasma Phys. Control. Fusion 45 (2003) 1627;
W. Fundamenski et al., Plasma Phys. Control. Fusion 46 (2004) 233.
[3] P.B. Snyder et al., Phys. Plasmas 9 (2002) 2037.
[4] M.E. Fenstermacher et al., Plasma Phys. Control. Fusion 45 (2003) 1597.
[5] W. Suttrop, Plasma Phys. Control. Fusion 42 (2000) A1.
[6] A. Loarte et al., Plasma Phys. Control. Fusion 45 (2003) 1549.
[7] G. Wang et al., Rev. Sci. Instrum., in press.
[8] L. Zeng et al., Rev. Sci. Instrum. 74 (2003) 1530.
[9] L. Zeng, Plasma Phys. Control. Fusion 46 (2004) A121.
[10] L. Zeng et al., in: Proceedings of the 6th International Reflectometry Workshop, 2003.
[11] T.E. Evans et al., Phys. Rev. Lett. 92 (2004) 235003.
[12] A.W. Leonard et al., Plasma Phys. Control. Fusion 44 (2002) 945.
[13] C.P. Perez et al., Nucl. Fusion 44 (2004) 609.
[14] J.A. Boedo et al., Phys. Plasmas, submitted for publication.
[15] A.W. Leonard et al., Phys. Plasma 10 (2003) 1765.
[16] P. Snyder et al., Plasma Phys. Control. Fusion 46 (2004) A131.